4-30-2019

Capillary penetration method for measuring wetting properties of carbon ionomer films for proton exchange membrane fuel cell (PEMFC) applications

Sofyane Abbou
Michigan Technological University, sabbou@mtu.edu

Kazuya Tajiri
Michigan Technological University, ktajiri@mtu.edu

K. T. Alofari
Michigan Technological University

Ezequiel F. Medici
Michigan Technological University, efmedici@mtu.edu

A. T. Haug
3M Company

See next page for additional authors

Recommended Citation

Abbou, S., Tajiri, K., Alofari, K. T., Medici, E. F., Haug, A. T., & Allen, J. S. (2019). Capillary penetration method for measuring wetting properties of carbon ionomer films for proton exchange membrane fuel cell (PEMFC) applications. *Journal of the Electrochemical Society, 166*(7), F3227-F3233. http://dx.doi.org/10.1149/2.0271907jes

Retrieved from: https://digitalcommons.mtu.edu/michigantech-p/268

Follow this and additional works at: https://digitalcommons.mtu.edu/michigantech-p

 Part of the Mechanical Engineering Commons

JES Focus Issue on Advances in Modern Polymer Electrolyte Fuel Cells in Honor of Shimshon Gottesfeld

Capillary Penetration Method for Measuring Wetting Properties of Carbon Ionomer Films for Proton Exchange Membrane Fuel Cell (PEMFC) Applications

S. Abbou,[1,*,z] K. Tajiri,[1] K. T. Alofari,[1] E. F. Médici,[1] A. T. Haug,[2] and J. S. Allen[1,*]

[1]*Department of Mechanical Engineering-Engineering Mechanics, Michigan Technological University, Houghton, Michigan 49931, USA*
[2]*3M Company, 3M Center, St. Paul, Minnesota 55144, USA*

In this work, capillary rise experiments were performed to assess the wetting properties of carbon-ionomer (CI) films. The samples were attached to a micro-balance and then immersed into liquid water to (i) measure the mass gain from the liquid uptake and (ii) estimate the (external) contact angle to water (typical value around 140°). The results showed that drying the CI films under low vacuum significantly impacted the CI film wettability. The influence of the ionomer content on the CI films' wettability was investigated with various ionomer to carbon (I/C) ratios: 0.8, 1.0, 1.2 and 1.4. No significant variation of the contact angle to water extracted from the capillary rise experiment was measured. However, water uptake increased with the I/C ratio suggesting a more hydrophilic behavior. This observation was in good agreement with the measurement from the sessile drop method showing a slight decrease of the contact angle to water: from 155° for an I/C of 0.8 to 135° for I/C = 1.4.
 [DOI: 10.1149/2.0271907jes]

Manuscript submitted November 21, 2018; revised manuscript received April 9, 2019. Published April 30, 2019. This was Paper 1421 presented at the National Harbor, Maryland Meeting of the Society, October 1–5, 2017. *This paper is part of the JES Focus Issue on Advances in Modern Polymer Electrolyte Fuel Cells in Honor of Shimshon Gottesfeld.*

In a Proton Exchange Membrane Fuel Cell (PEMFC), inappropriate water management may lead to performance losses[1–3] and irreversible electrode degradation.[4–9] Therefore, designing materials with proper hydrophobicity is crucial in mitigating flooding issues.

Previous research has focused on investigating the effect of gas diffusion layer (GDL) hydrophobicity on PEMFC performance. The wetting properties of the GDLs were approximated or measured using experimental methods such as goniometry (e.g., sessile drop technique),[10] capillary rise[11] and Wilhelmy plate[11] to determine the external contact angle to water. Capillary penetration techniques (e.g., Washburn method) have also been used to understand the relationship between pore structure, internal wettability and capillarity.[11–15] Percolation tests led to a better understanding of the water transport mechanisms in the GDLs based on the capillary phenomena.[16,17] Based on those experimental investigations, diverse models, including the pore network model developed by Médici and Allen,[18–21] offered an accurate prediction of liquid water distribution within the GDLs: see literature reviews[22,23] and references therein. All these studies have provided useful information to improve water management issues. However, only few experimentally explored the effect of the catalyst layer (CL) wettability on water management.

CL wettability may be tuned by changing the porous structure or the surface chemistry. Extensive work done by Professor Xie's group showed that carbon support functionalization with hydrophilic groups improved the water retention in the cathode catalyst layer.[24–26] The results also highlighted the benefits of catalyst functionalization on fuel cell performance and durability. Li et al.[27] investigated the effects of cathode CL hydrophobicity on the fuel cell performance. They demonstrated that the addition of dimethyl silicone oil (DSO) during the ink preparation increased the CL surface contact angle to water as measured using the sessile drop technique. Single cell tests revealed that an optimized DSO loading in the cathode CL helped prevent cathode flooding at high current density. Other researchers achieved similar results by adding polytetrafluoroethylene (PTFE),[28] fluorinated ethylene propylene (FEP) nanoparticles[29] or polydimethylsiloxane (PDMS)[30] in the CL. However, the incorporation of hydrophobic agents into the CLs may reduce the pore space and/or cover the Pt particles lowering electronic and protonic conductivities.[31] Yu et al.[32] studied the wetting properties of catalyst layers with different pore size distributions. They combined conventional contact angle measurement with microstructure analyses, porosity measurements and energy dispersive X-Ray analysis (EDX). They found that the microstructure and the local composition of the CL has a significant impact on the contact angle to water (values ranging from 140° to 150°). To date, however, little attention has been paid to the liquid water/ionomer interactions.

In this work we designed a simple measurement technique based on the capillary penetration method for the simultaneous evaluation of liquid water uptake and contact angle for hydrophobic carbon-ionomer (CI) films (i.e., electrodes without catalyst) provided by the 3M Company. As the ionomer morphology is known to depend on the sample thermal history,[33] we investigated the impact of different sample preparation protocols on CI films wettability. Samples with several ionomer to carbon ratios were also tested to better understand the ionomer influence on water transport.

Experimental

Sample preparation.—The CI films tested in this work consisted of Vulcan XC-72 carbon (surface area of 250 m^2/g) dispersed in a 3M brand ionomer matrix (equivalent weight -EW- of 825) with an ionomer to carbon (I/C) ratio of 0.8 and a carbon areal weight of 0.4 mg_C/cm^2. The CI films were freestanding layers deposited on a removable liner; meaning that they were not attached to any membrane nor GDL layers. Being very thin (about 8 μm on scanning electron microscope – SEM – images), the CI films were not stiff enough to immerse directly into the liquid as required by the capillary penetration measurement described in Capillary penetration measurement section. Therefore, each sample was prepared by hot-pressing the CI films for 15 minutes (20 bar, 145°C) on both sides of an Ethylene Tetrafluoroethylene (ETFE) substrate with the following dimensions: 3 cm high, 2 cm wide and 120 μm thick. After the hot-pressing step, the samples (i.e., CI films on both sides of ETFE) were cooled down at room temperature for 5 to 10 minutes before testing.

ETFE was chosen as a substrate based on preliminary data, not presented here, showing that the ETFE film didn't absorb any water when immersed into water. The hot-press used in this work was a Carver model C (Fred S. Carver Inc., IN, USA).

*Electrochemical Society Member.
[z]E-mail: abbou.sofyane@gmail.com

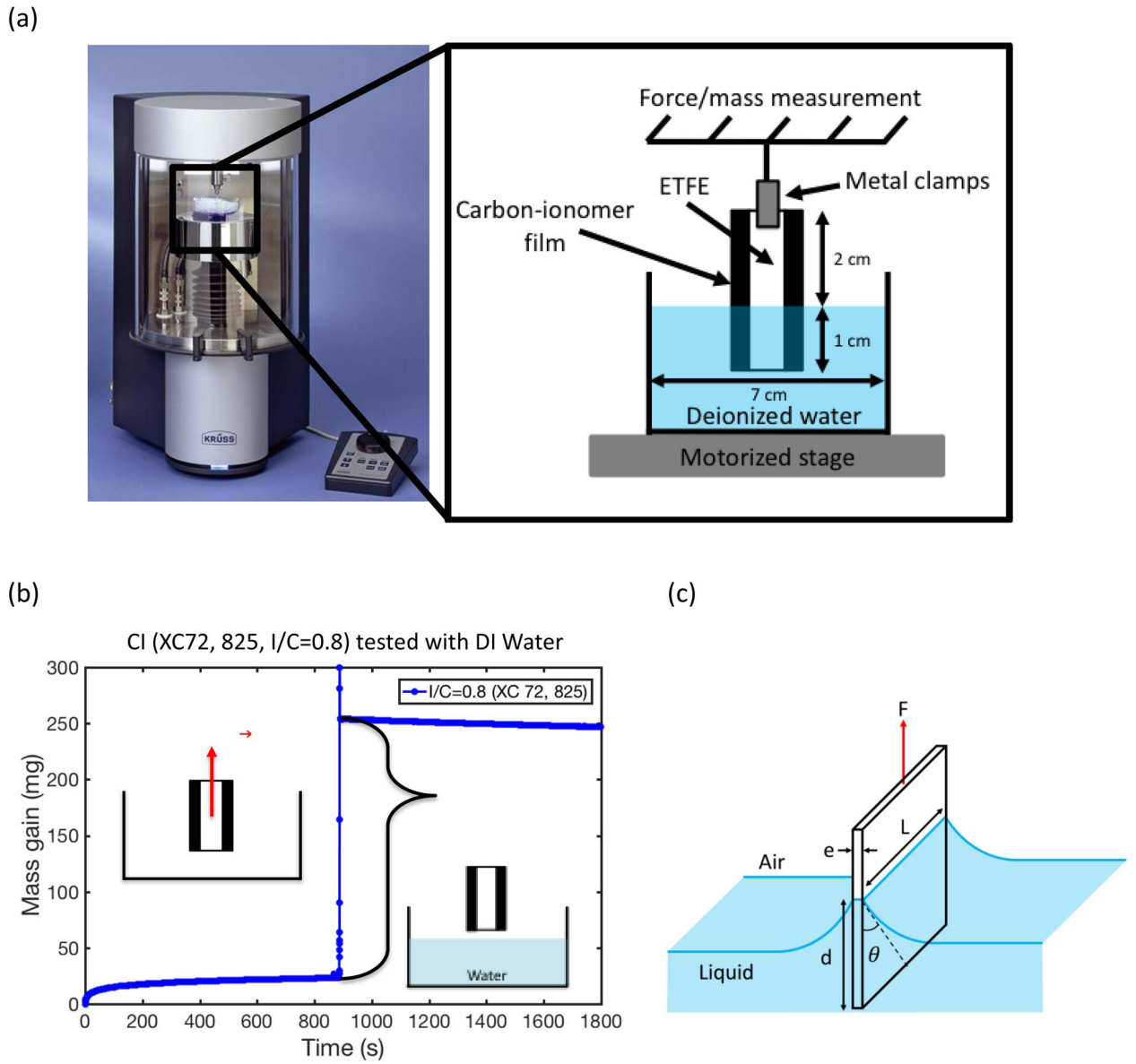

Figure 1. (a) Krüss tensiometer K100 (Krüss GmbH, Hamburg, Germany) used to measure the mass evolution of CI films. Before testing, the CI films were hot-pressed on both sides of an ETFE film: 3 cm high; 2 cm wide and 120 μm thick. (b) Mass evolution of a CI film (XC-72, EW 825, I/C = 0.8) during the capillary rise experiment we designed. The contact angle to water estimated using the method described in this section was found equal to 139°. (c) Illustration of Wilhelmy plate method: the magnitude of the capillary force F on the plate is proportional to the wetted perimeter, and to the surface tension of the water-air interface.

Capillary penetration measurement.—As described in our previous works,[34,35] the tests were performed using a Krüss force tensiometer K100 (Krüss GmbH, Hamburg, Germany) operated in the absorption mode (Figure 1a). After the hot-pressing step described in the Sample preparation section, the samples (CI films on both side of an ETFE substrat) were suspended from the top of the instrument's microbalance. Deionized (DI) water at room temperature was placed on a motorized platform. The sample was then immersed 1 cm into the water at a constant speed of 10 cm/min. The increase in sample mass due to the added liquid weight was determined with respect to time during the measurement.

To estimate the contact angle, the vessel containing the water was removed after 900 seconds which causes a sudden increase in the mass detected by the micro balance (see Figure 1b). The change in the measured mass (Δm in Figure 1b and Equation 2) was used to estimate the wetting force exerted on the sample and thus the external contact angle to water. Indeed, when a sample is immersed into the liquid, the force exerted on it due to wetting is given by the Wilhelmy equation:

$$\gamma = \frac{F}{2\,(L + e)\cos\theta} \qquad [1]$$

where γ is the surface tension (taken as 72 mN/m), L is the sample width (2 cm), e is the sample thickness (140 μm), d the immersion depth (1 cm), θ is the contact angle between the liquid phase and the sample and F the force exerted on the sample (N). The force F can be estimated from the energy released when the sample was pulled out from the liquid (at t = 900s in Figure 1b) and corrected for buoyancy, which was in our case an order of magnitude less than the weight. Therefore, the force F can be expressed as following:

$$F = -\,\Delta m.g + \rho_l g V_i \qquad [2]$$

with Δm the mass difference (kg) before and after the sample was removed from the liquid (at t = 900 s.), g is the gravitational constant,

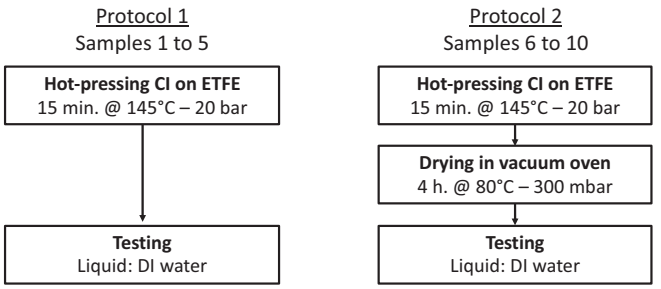

Figure 2. Flow chart illustrating the preparation protocols developed to assess the effect of heat-treatment prior to testing on CI films' wettability. Protocol 1: samples #1 to #5 were tested immediately after the hot-pressing with ETFE. Protocol 2: samples #5 to #10 were dried during under low vacuum prior to testing.

ρ_l is the liquid density (998 kg/m^3) and V_i the fraction of the sample immersed into the liquid with $V_i = Led$.

By combining Equations 1 and 2, the (external) contact angle can be expressed as:

$$\theta = \cos^{-1}\left(\frac{-\Delta m.g + \rho_l g V_i}{2(L+e)\gamma}\right) \quad [3]$$

Sessile drop measurement.—To complete our observations and to confront the estimation of contact angle made using Equation 3, the external contact angles of the CI films were also measured using the more conventional sessile drop method performed at room temperature. The drops were generated using a 1750 TPLT Hamilton Gastight 500 µL syringe. A Kodak Medalist AF Carousel Projector was used as a light source along with an Edmund Industrial Optics microscope. The images were captured using a high resolution Pulnix, TM-1325CL CCD camera. The contact angles were calculated from image analysis using an open access software: Image J.

Results and Discussion

Effect of heat-treatment before testing.—Two sample preparation protocols were used to investigate the effect of heat-treatment on wetting properties of the CI films (Figure 2). For both protocols, five different samples were prepared by hot-pressing CI films (XC-72, EW 825, I/C = 0.8) on both sides of an ETFE substrate. For protocol 1, samples #1 to #5 were tested with DI water immediately after the hot-pressing. For protocol 2, samples #5 to #10 were, prior to testing, dried for 4 hours at 80°C and 300 mbar under the atmospheric pressure in a Precision vacuum oven model 19 (Precision Scientific Inc., IL, USA). For both protocols, the corresponding water uptakes and average contact angles to water are respectively given in Figure 3 and Table I.

Figure 3 shows the mass evolution of samples tested for both protocols. For protocol 1 (samples #1 to #5), no significant variation was observed: the average mass gain after 900 seconds was 14 mg with a 10% relative standard deviation (RSD). The contact angles to water were very consistent for this protocol with an average value of 143° and an RSD of 5%. For protocol 2, a significant dispersion in the mass gain was observed with an RSD of 32%. The contact angles to water

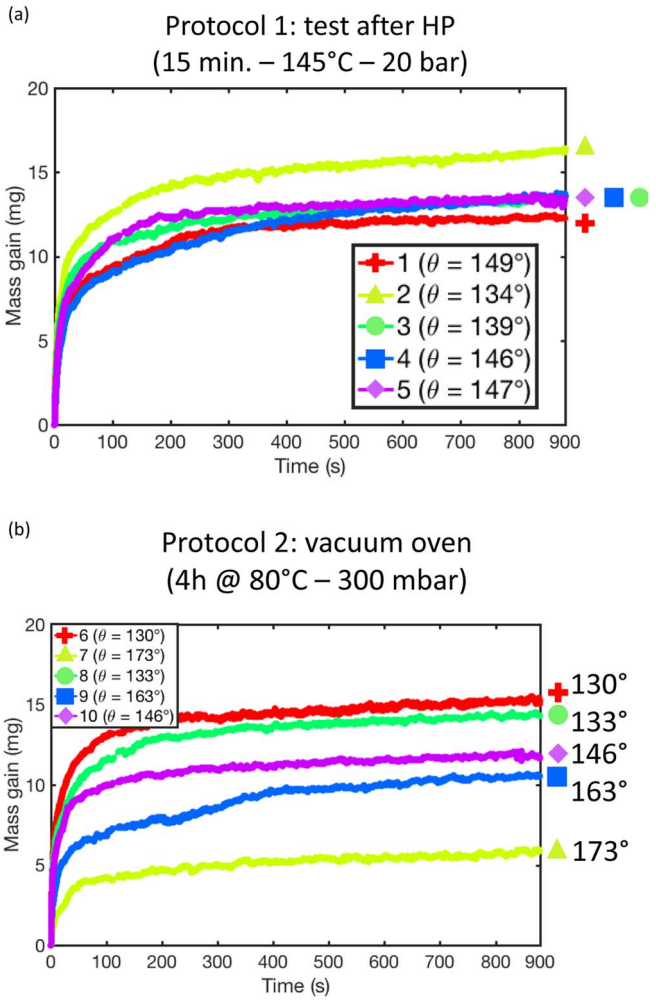

Figure 3. Time evolution of the gain in mass for CI films tested through protocols 1 and 2. (a) Samples #1 to #5 were tested directly after the hot-pressing step (protocol 1, Figure 2). (b) Samples #6 to #10 were dried under low vacuum prior to testing. For both protocols, the average water uptakes and contact angles to water are given in Table I.

ranged from 130° to 173° with an average value of 149° and RSD of 17%. These results indicate that the wetting properties of the CI films were strongly affected by the drying step under low vacuum. As a possible explanation, the drying process in the vacuum oven may have altered ionomer structure and morphology within the CI films and thus the sample wetting properties.[33]

Drying procedures after testing.—In order to find an efficient way to dry the samples and evaporate the residual liquid water absorbed from the prior measurement, two samples (#11 and #12) were prepared by hot-pressing CI films (XC-72, 825, I/C = 0.8) on both sides of ETFE (15 minutes at 145°C and 20 bar). Protocol 3, sample #11 was successively tested and dried in the hot-press during 15 minutes at

Table I. Average values and relative standard deviations (RSD) for contact angles to water and mass gains after 900 seconds for protocols 1 and 2 (see also Figure 3).

	Mass gain after 900s		Contact angle to water	
Protocol	Average (mg)	RSD (%)	Average (°)	RSD (%)
#1 Test after hot-pressing Samples 1–5	14	10	143	5
#2 Drying in vacuum oven Samples 6–10	10	32	149	17

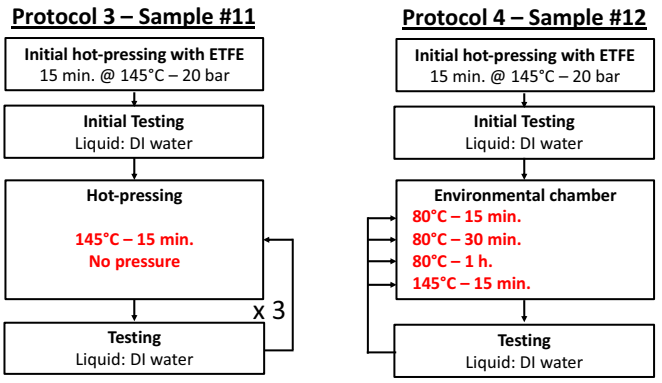

Figure 4. Flow chart illustrating the drying protocols 3 and 4. Protocol 3, sample #11 was successively tested and dried using the hot-press (15 minutes at 145°C with no pressure); this sequence was repeated 3 times. Protocol 4, sample #12 was dried using an environmental chamber. After each test we varied the drying conditions as follows: 15 minutes at 80°C, 30 minutes at 80°C, 1 hour at 80°C and 15 minutes at 145°C. For both protocols, the corresponding water uptakes are given in Figure 5.

145°C; no pressure was applied in order to avoid sample deformation (Figure 4). This sequence was repeated 3 times in total and the first test is referred to as 'initial test' (red curves, Figure 5). Protocol 4, sample #12 was successively tested and dried using a Tenney Jr. environmental chamber. Beside the 'initial test', sample #12 was tested 4 additional times. After each test, we changed the drying conditions (temperature and/or duration) as follows:

- 15 minutes at 80°C;
- 30 minutes at 80°C;
- 1 hour at 80°C;
- 15 minutes at 145°C (conditions similar to the hot-pressing).

Figure 5 shows the mass evolutions of samples #11 and #12. For sample #11, very consistent liquid uptakes were obtained after the successive drying in the hot-press (Figure 5a). This observation suggest that the residual water was effectively removed between each test.

For sample #12, the liquid uptakes were strongly affected by the drying conditions (Figures 5b and 5c). After the sample was dried 15 minutes at 80°C, the mass gain after 900 seconds was less than 40% relative to the mass gain measured at the end of the initial test (red curve in Figure 5b). This observation suggests that the sample still contained a significant amount of residual water from the prior test. A slight increase in the liquid uptake was observed when the sample was tested after being dried for 30 minutes at 80°C: the mass gain after 900 seconds relative to the initial test was above 50%. After being dried for 1 hour at 80°C, the mass evolution started to approximate the one obtained for the initial test by reaching 90% of its value. After 15 minutes at 145°C, the mass gain after 900 seconds reached 98% of the initial test's mass gain.

Based on these results, hot-pressing (15 min at 145°C) appears to be a good way to dry the samples before testing. No additional drying step prior to testing is required. An efficient removal of the residual water from the sample (≥90%) may also be achieved using a more conventional environmental chamber at low (1 h. – 80°C) or high (15 min. – 145°C) temperatures.

The results presented in Effect of heat treatment before testing and Drying procedures after testing sections allowed us to put in place a reliable sample preparation protocol that provides consistent and repeatable results and set a standard baseline for our testing protocol. In the final section, we investigate the influence of the I/C ratio on CI film wetting properties.

Influence of the I/C ratio.—The influence of the ionomer content on wetting properties was investigated for CI films (carbon Vulcan XC-72, 3M ionomer EW 825) with four different I/C (mass) ratios: 0.8, 1.0, 1.2 and 1.4. The same mass of carbon was used for all samples and the amount of ionomer was adjusted to meet the desired I/C ratio. The average CI film thickness measured using SEM images was 8 μm with a standard deviation between each sample within 15%. Before being immersed into water, each sample was first hot-pressed on both sides of a 120 μm ETFE substrate (15 minutes – 145°C – 20 bar). The corresponding liquid uptakes and contact angles to water are presented in Figure 6.

Figure 6 shows the liquid uptakes of CI films with different I/C ratios. The difference between sample thickness (i.e., volume) remained within 15%. The total mass gain after 900 seconds ranged from 9 mg at I/C = 0.8 to 18 mg at I/C = 1.4. The Figure 6b shows the mass increase corrected by the I/C ratio with a logarithmic scale in the time axis. All the curves have a similar slope and seem to align very well. This result suggest that the water was mainly absorbed by the ionomer phase and the pore space had a limit influence in water uptake in the I/C range explored in this work. From the slopes, this method made it possible to capture the intrinsic liquid water absorption rate by the ionomer in the porous CI films.

Figure 7 shows the contact angle measured by (i) the capillary penetration method (blue dots) and (ii) sessile drop technique (red squares). The results from the sessile drop (red squares) showed a slight decrease of the contact angle with the I/C ratio: the contact angle was 20° smaller when the I/C ratio was increased from 0.8 to 1.4. This result indicates that the samples were more hydrophilic at higher I/C ratio which is consistent with the liquid uptake shown in Figure 6. However, no clear variation of the contact angles with the I/C ratio was observed from the capillary rise method (blue dots). For instance, we observed an unexpected increase of the contact angle at I /C = 1.2.

Overall, the contact angle estimated with the capillary penetration method are in good agreement with the sessile drop results. For the latter, the results were more consistent since they mostly depend on the surface roughness. However, for the contact angle estimated using the capillary rise method, the uncertainties were much higher: standard deviations ranging from 4° to 8° (see Table II). Most likely, non-homogenous sample thickness and/or ionomer dispersion may affect water uptake and *in fine* induce significant discrepancies in the contact angle estimated using Equation 3. At I/C = 1.2, the standard deviation associated with the contact angle estimated with capillary rise method was ±8°; which made it difficult to detect small changes in the contact angle when compared to other samples at different I/C ratios. As a drawback, the capillary rise experiment is not well suited to capture variation in contact angle lower than 10°. Nevertheless, we recently showed that the effect of ionomer chemistry on contact angle can be assessed using this methodology.[35]

Conclusions

In this work, a simple capillary rise experiment was designed to (i) measure the water uptake and (ii) estimate the (external) contact angle to water of carbon-ionomer films (i.e., electrodes without catalyst) provided by the 3M Company. The results showed that inappropriate heat-treatment may affect the wetting properties of CI films. Drying the samples in a vacuum oven prior to testing led to a high disparity in the liquid uptake for different samples with same specifications: carbon XC-72, ionomer EW 825 with I/C of 0.8. Such inconsistency was not observed when the samples were tested directly after the initial hot-pressing step with ETFE. Successive drying/testing cycles showed that exposure to high temperature (15 min. at 145°C) during the hot-pressing step was an efficient way to remove the residual water from prior testing. Effective drying may also be achieved using a more conventional environmental chamber under similar conditions (i.e., 15 min. at 145°C) or at lower temperature (i.e., 80°C) providing the appropriate duration (at least 1 hour in our case).

The influence of the ionomer content was investigated using carbon-ionomer films with various I/C ratios: 0.8, 1.0, 1.2 and 1.4. The contact angles measured using the sessile drop method showed a slight decrease of the contact angle with the I/C ratio. This obser-

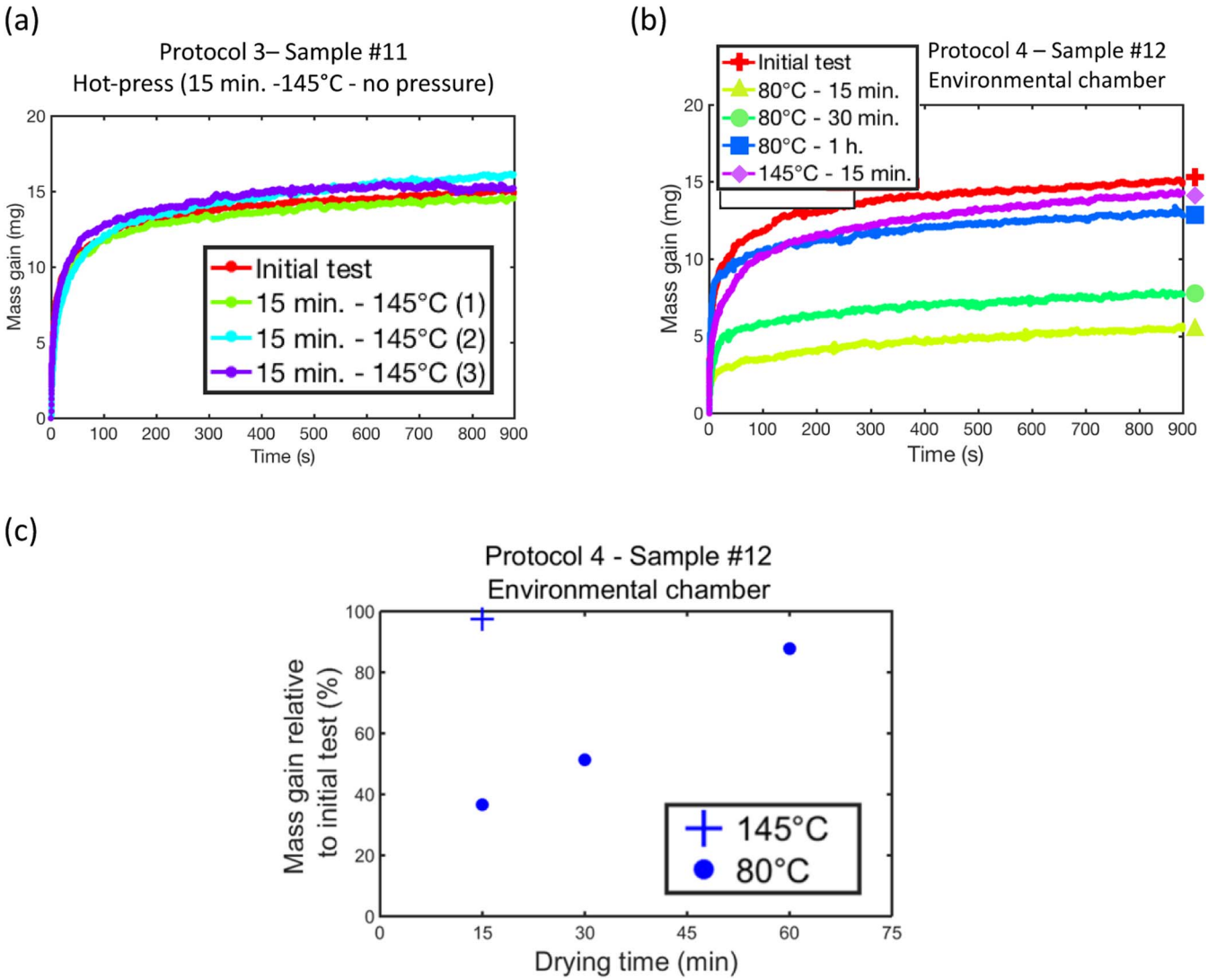

Figure 5. Time evolution of the gain in mass for samples #11 and #12. (a) Protocol 3, sample #11 was successively tested and dried using the hot-press (15 minutes at 145°C). (b) Protocol 4, sample #12 was dried using an environmental chamber. Between each test, we changed the drying conditions as follows: 80°C – 15 min., 80°C –30 min., 80°C – 1 h and 145°C – 15 min. The red curves referred as 'initial test' were obtained immediately after the initial hot-pressing steps with ETFE. (c) Mass gain (in %) relative to the initial test versus the drying time in the environmental chamber for protocol 4 (sample #12); the mass gain of the initial test (red curve in Figure 5b) was set at 100%.

vation reflects a more hydrophilic behavior which is consistent with the liquid uptake measurements. As a drawback, the contact angle estimated from the capillary rise experiments were unable to capture such a small variation of contact angle for the I/C ratios considered in this work due to the large uncertainties (up to ± 8°).

Thus, we proposed a simple technique that has the potential to capture dynamic information of (a) contact angle, (b) ionomer water uptake and (c) surface energy all in one single test. In the future, carbon-ionomer films with a wider range of I/C ratios will be tested. The influence of the ionomer chemistry on electrode wetting properties will also be investigated. Coupling Owens-Wendt analysis and capillary rise experiments may be used to extract the sample surface energy and the internal contact angle.[11,12] To annihilate the possible effect of the hot-pressing step on the ionomer structure and morphology, the CI films will be directly coated on the both side of the ETFE film during the manufacturing process.

Table II. Contact angle to water and mass gain after 900 seconds for CI films with I/C ratios of 0.8, 1.0, 1.2 and 1.4 (see also Figure 6). The average CI film thickness was 8 μm with a standard variation between each sample within 15%.

		Contact angle to water (°)	
XC-72, EW 825 I/C ratio	Mass gain after 900 s. (mg)	Capillary rise	Sessile drop
0.8	9	146 ± 6°	155 ± 2°
1.0	12	139 ± 5°	148 ± 2°
1.2	16	148 ± 8°	144 ± 2°
1.4	18	137± 4°	135 ± 2°

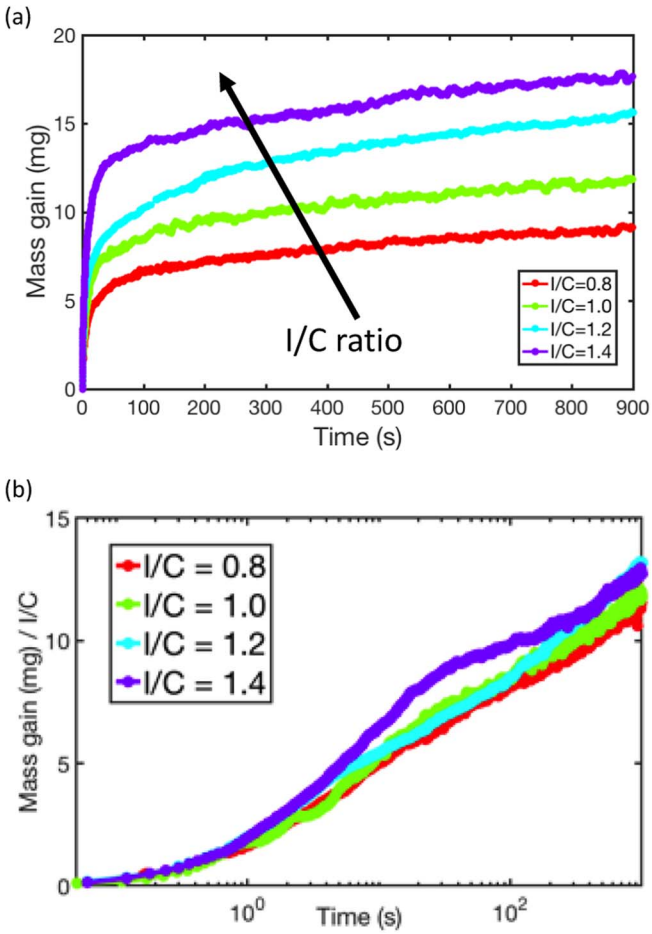

Figure 6. (a) Time evolution of the gain in mass for carbon-ionomer films with I/C ratios of 0.8, 1.0, 1.2 and 1.4. All the samples were hot-pressed with ETFE. (b) Gain in mass corrected by the I/C ratio with a logarithmic scale in the time axis.

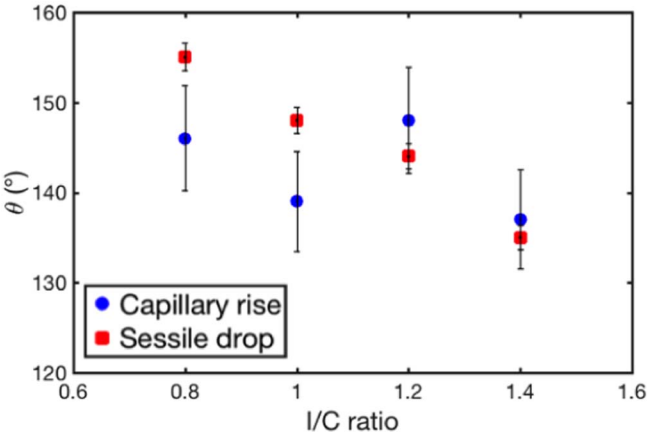

Figure 7. Contact angle to water as a function of the I/C ratio. The contact angles were determined by calculating the capillary force when the samples were pulled out the water at t = 900s (see Appendix A). For each I/C ratio, the average contact angle (and standard deviation) of 3 different samples was plotted. Those values were compared to the ones measured using the sessile drop technique (± 2°) with similar materials.

Acknowledgments

This material is based upon work supported by the Department of Energy, Office of Energy Efficiency and Renewable Energy (EERE), under Award Number DE-EE0007270. This report was prepared as an account of work sponsored by an agency of the United States Government. Neither the United States Government nor any agency thereof, nor any of their employees, makes any warranty, express or implied, or assumes any legal liability or responsibility for the accuracy, completeness, or usefulness of any information, apparatus, product, or process disclosed, or represents that its use would not infringe privately owned rights. Reference herein to any specific commercial product, process, or service by trade name, trademark, manufacturer, or otherwise does not necessarily constitute or imply its endorsement, recommendation, or favoring by the United States Government or any agency thereof. The views and opinions of authors expressed herein do not necessarily state or reflect those of the United States Government or any agency thereof.

ORCID

S. Abbou https://orcid.org/0000-0001-6221-6411

References

1. U. N. Shrivastava, K. Tajiri, and M. Chase, "Current density and ohmic resistance distribution in the land-channel direction of a proton exchange membrane fuel cell," *J. Power Sources*, **299**, 189 (2015).
2. U. N. Shrivastava and K. Tajiri, "In-Plane Distribution Analysis in the Land-Channel Direction of a Proton Exchange Membrane Fuel Cell (PEMFC)," *J. Electrochem. Soc.*, **162**(7), F722 (2015).
3. U. N. Shrivastava and K. Tajiri, "Sources of Current Density Distribution in the Land-Channel Direction of a PEMFC," *J. Electrochem. Soc.*, **163**(9), F1072 (2016).
4. L. Dubau et al., "Carbon corrosion induced by membrane failure: The weak link of PEMFC long-term performance," *Int. J. Hydrog. Energy*, **39**(36), 21902 (2014).
5. S. Abbou et al., "High Potential Excursions during PEM Fuel Cell Operation with Dead-Ended Anode," *J. Electrochem. Soc.*, **162**(10), F1212 (2015).
6. S. Abbou, J. Dillet, G. Maranzana, S. Didierjean, and O. Lottin, "Local potential evolutions during proton exchange membrane fuel cell operation with dead-ended anode – Part I: Impact of water diffusion and nitrogen crossover," *J. Power Sources*, **340**(Supplement C), 337 (2017).
7. S. Abbou, J. Dillet, G. Maranzana, S. Didierjean, and O. Lottin, "Local potential evolutions during proton exchange membrane fuel cell operation with dead-ended anode – Part II: Aging mitigation strategies based on water management and nitrogen crossover," *J. Power Sources*, **340**(Supplement C), 419 (2017).
8. S. Abbou et al., "Time Evolution of Local Potentials during PEM Fuel Cell Operation with Dead-Ended Anode," *ECS Trans.*, **58**(1), 1631 (2013).
9. S. Abbou, J. Dillet, G. Maranzana, S. Didierjean, and O. Lottin, "Impact of Water Management on Local Potential Evolutions during PEM Fuel Cell Operation with Dead-Ended Anode," *ECS Trans.*, **69**(17), 1267 (2015).
10. M. Mortazavi and K. Tajiri, "Effect of the PTFE content in the gas diffusion layer on water transport in polymer electrolyte fuel cells (PEFCs)," *J. Power Sources*, **245**, 236 (2014).
11. D. L. Wood, C. Rulison, and R. L. Borup, "Surface Properties of PEMFC Gas Diffusion Layers," *J. Electrochem. Soc.*, **157**(2), B195 (2010).
12. V. Gurau, M. J. Bluemle, E. S. De Castro, Y.-M. Tsou, J. A. Mann, and T. A. Zawodzinski, "Characterization of transport properties in gas diffusion layers for proton exchange membrane fuel cells: 1. Wettability (internal contact angle to water and surface energy of GDL fibers)," *J. Power Sources*, **160**(2), 1156 (2006).
13. V. Gurau and J. A. Mann, "Technique for characterization of the wettability properties of gas diffusion media for proton exchange membrane fuel cells," *J. Colloid Interface Sci.*, **350**(2), 577 (2010).
14. B. R. Friess and M. Hoorfar, "Measurement of internal wettability of gas diffusion porous media of proton exchange membrane fuel cells," *J. Power Sources*, **195**(15), 4736 (2010).
15. V. Parry, E. Appert, and J.-C. Joud, "Characterisation of wettability in gas diffusion layer in proton exchange membrane fuel cells," *Appl. Surf. Sci.*, **256**(8), 2474 (2010).
16. E. F. Medici and J. S. Allen, "Existence of the phase drainage diagram in proton exchange membrane fuel cell fibrous diffusion media," *J. Power Sources*, **191**(2), 417 (2009).
17. E. F. Médici and J. S. Allen, "Scaling percolation in thin porous layers," *Phys. Fluids*, **23**(12), 122107 (2011).
18. E. F. Medici and J. S. Allen, "The Effects of Morphological and Wetting Properties of Porous Transport Layers on Water Movement in PEM Fuel Cells," *J. Electrochem. Soc.*, **157**(10), B1505 (2010).
19. E. F. Médici and J. S. Allen, "Evaporation, two phase flow, and thermal transport in porous media with application to low-temperature fuel cells," *Int. J. Heat Mass Transf.*, **65**, 779 (2013).
20. I. V. Zenyuk, E. Medici, J. Allen, and A. Z. Weber, "Coupling continuum and pore-network models for polymer-electrolyte fuel cells," *Int. J. Hydrog. Energy*, **40**(46), 16831 (2015).

21. E. F. Medici, I. V. Zenyuk, D. Y. Parkinson, A. Z. Weber, and J. S. Allen, "Understanding Water Transport in Polymer Electrolyte Fuel Cells Using Coupled Continuum and Pore-Network Models," *Fuel Cells*, **16**(6), 725 (2016).
22. M. Secanell, A. Jarauta, A. Kosakian, M. Sabharwal, and J. Zhou, "PEM Fuel Cells, Modeling," in *Encyclopedia of Sustainability Science and Technology*, R. A. Meyers, Ed. New York, NY: Springer New York, 2017, pp. 1.
23. A. Z. Weber et al., "A Critical Review of Modeling Transport Phenomena in Polymer-Electrolyte Fuel Cells," *J. Electrochem. Soc.*, **161**(12), F1254 (2014).
24. M. Wang et al., "Enhancing the Catalytic Performance of Pt/C Catalysts Using Steam-Etched Carbon Blacks as a Catalyst Support," *ECS Trans.*, **33**(1), 507 (2010).
25. F. Xu et al., "Enhanced Pt/C catalyst stability using p-benzensulfonic acid functionalized carbon blacks as catalyst supports," *Electrochimica Acta*, **94**, 172 (2013).
26. L. Xin et al., "Enhanced MEA Performance for PEMFCs under Low Relative Humidity and Low Oxygen Content Conditions via Catalyst Functionalization," *J. Electrochem. Soc.*, **164**(6), F674 (2017).
27. A. Li, M. Han, S. H. Chan, and N. Nguyen, "Effects of hydrophobicity of the cathode catalyst layer on the performance of a PEM fuel cell," *Electrochimica Acta*, **55**(8), 2706 (2010).
28. B. Chi et al., "Tuning hydrophobic-hydrophilic balance of cathode catalyst layer to improve cell performance of proton exchange membrane fuel cell (PEMFC) by mixing polytetrafluoroethylene (PTFE)," *Electrochimica Acta*, **277**, 110 (2018).
29. G. S. Avcioglu, B. Ficicilar, and I. Eroglu, "Influence of FEP nanoparticles in catalyst layer on water management and performance of PEM fuel cell with high Pt loading," *Int. J. Hydrog. Energy*, **42**(1), 496 (2017).
30. M. Choun, D. Nauryzbayev, D. Shin, and J. Lee, "Polydimethylsiloxane treated cathode catalyst layer to prolong hydrogen fuel cell lifetime," *Catal. Today*, **262**, 155 (2016).
31. G. S. Avcioglu, B. Ficicilar, and I. Eroglu, "Effective factors improving catalyst layers of PEM fuel cell," *Int. J. Hydrog. Energy*, (2018).
32. H. M. Yu, C. Ziegler, M. Oszcipok, M. Zobel, and C. Hebling, "Hydrophilicity and hydrophobicity study of catalyst layers in proton exchange membrane fuel cells," *Electrochimica Acta*, **51**(7), 1199 (2006).
33. A. Kusoglu and A. Z. Weber, "New Insights into Perfluorinated Sulfonic-Acid Ionomers," *Chem. Rev.*, **117**(3), 987 (2017).
34. S. Abbou, K. Tajiri, E. Medici, and J. S. Allen, "Characterization of Water Transport in PEMFC Electrode Using the Washburn Method," *ECS Trans.*, **80**(8), 87 (2017).
35. S. Abbou, K. Tajiri, E. Medici, A. T. Haug, and J. S. Allen, "Liquid Water Uptake and Contact Angle Measurement of Proton Exchange Membrane Fuel Cell (PEMFC) Electrodes," *ECS Trans.*, **86**(13), 163 (2018).